Numerical Investigation of Nonlinear Internal Wave Generation and Breaking in Straits

Sonya Legg
Atmosphere and Ocean Sciences Program
Princeton University, Sayre Hall, Forrestal Campus
300 Forrestal Drive
Princeton NJ 08544
phone: (609) 253-6852 fax: (609) 987-5063 email: Sonya.Legg@Noaa.gov

Award Number: N000140910832

LONG-TERM GOALS

Our long-term goals are to develop a physical understanding of the processes which lead to mixing in the ocean, with the aim of using this understanding to develop parameterizations of mixing suitable for global and regional models, and applying such models to societally relevant problems. A particular focus is the mixing induced by tidal flow over topography, and mixing induced by breaking nonlinear internal waves.

OBJECTIVES

The scientific objectives of this study are to explore internal waves generated by tidal flow through straits in the region close to the sill. Our geographic focus is the Luzon Straits. A particular scientific focus is nonlinear overturning and breaking within the straits leading to mixing and modification of the wave field. One possibility which we examine is whether transient internal hydraulic jumps are possible in the Luzon Straits, whether these jumps are released to propagate toward the topography as internal bores when the flow relaxes, and whether the bores lead to local mixing. We will explore the details of the Luzon Strait topography to identify locations particularly conducive to local overturning processes. The Luzon Strait features two parallel north south oriented ridges. We will examine how the wave fields of the two ridges interact and affect wave generation and mixing processes. We will also examine the importance of three-dimensional bathymetry in determining the locations of mixing. The sensitivity of the nonlinear wave response to the local stratification near the sill, and the ambient geostrophic currents will be examined. To summarize, our goals are to (a) examine the dependence of nonlinear features and local breaking at the generation site on topographic shape and stratification; (b) evaluate how the interaction between the ridges affect the mixing; (c) examine the extent to which the mixing processes are determined by three-dimensional topography variations, and (d) examine the impact of seasonal variations in stratification and geostrophic currents on the length-scales and amplitude of the internal tides.

APPROACH

We employ the nonhydrostatic MITgcm in both 2- and 3-dimensions to carry out simulations of increasing complexity, focusing the resolution on the regions close to the sill where overturning is

Report Documentation Page

Form Approved
OMB No. 0704-0188

1. REPORT DATE
30 SEP 2011

2. REPORT TYPE

3. DATES COVERED
00-00-2011 to 00-00-2011

4. TITLE AND SUBTITLE
Numerical Investigation of Nonlinear Internal Wave Generation and Breaking in Straits

5a. CONTRACT NUMBER

5b. GRANT NUMBER

5c. PROGRAM ELEMENT NUMBER

6. AUTHOR(S)

5d. PROJECT NUMBER

5e. TASK NUMBER

5f. WORK UNIT NUMBER

7. PERFORMING ORGANIZATION NAME(S) AND ADDRESS(ES)
Princeton University,Atmosphere and Ocean Sciences Program,300 Forrestal Drive,Princeton,NJ,08544

8. PERFORMING ORGANIZATION REPORT NUMBER

9. SPONSORING/MONITORING AGENCY NAME(S) AND ADDRESS(ES)

10. SPONSOR/MONITOR'S ACRONYM(S)

11. SPONSOR/MONITOR'S REPORT NUMBER(S)

12. DISTRIBUTION/AVAILABILITY STATEMENT
Approved for public release; distribution unlimited

13. SUPPLEMENTARY NOTES

14. ABSTRACT

15. SUBJECT TERMS

16. SECURITY CLASSIFICATION OF:			17. LIMITATION OF ABSTRACT	18. NUMBER OF PAGES	19a. NAME OF RESPONSIBLE PERSON
a. REPORT **unclassified**	b. ABSTRACT **unclassified**	c. THIS PAGE **unclassified**	**Same as Report (SAR)**	**8**	

most likely to occur. The MITgcm is well-suited for this study, having been used for numerous studies of nonlinear internal tides (e.g. Legg and Klymak, 2008). MITgcm is a *z*-coordinate model and it applies a simple vertical dissipation and mixing scheme that computes vertical viscosities and diffusivities computed by Thorpe sorting unstable density profiles (Klymak and Legg, 2010). Typical resolutions near the sill are O(100m) in the horizontal and O(10m) in the vertical. Most calculations have been performed on the NAVY cluster Da Vinci. Initial 3D simulations have focused on providing guidance for the main field program which took place in summer 2011, aiding observationalists Rob Pinkel and Jody Klymak in finding dissipation hotspots on top of the East Ridge in Luzon Strait. Following the field program, simulations will be carried out to help in interpretation of the observations, with increasing complexity, beginning with 2D simulations with horizontally uniform stratification, and proceeding to 3D simulations with complex realistic topography and ambient stratification. Most of the work is being carried out by Maarten Buijsman, a postdoctoral researcher based at Princeton, and we are collaborating closely with Jody Klymak. We are also communicating closely with other observationalists involved in the Luzon Straits field experiment.

WORK COMPLETED

Funding was awarded in spring of 2009, but Maarten Buijsman only joined the project in September 2010, so the major part of the work has been underway for a little more than a year. During this time we have completed a 2D study of the impact of topographic shape on the nonlinear waves, breaking and dissipation in the straits, comparing results with observations from the 2010 Luzon Straits pilot study. A 3D calculation has been completed for the purposes of guiding the observations in 2011 summer, and to examine the effect of 3D topography on the nonlinear waves and dissipation. The 2D model is run with realistic bathymetries including either a single West Ridge (WR), a single East Ridge (ER), or both ridges along a zonal transect in the central Luzon Strait, in order to understand the role of the double ridge topography. We refer to these model cases as reW, reE, and reWE, respectively. The 2D model has a minimal horizontal and vertical grid size of 100 m and 10 m. Figure 1 shows the bathymetry of case reWE. These simulations have the duration of a complete spring-neap cycle. This period covers the 24 hour observation stations N2a and N2b at the WR, during semidiurnal (D2) and diurnal (D1) tides, respectively (Alford et al 2011). The 3D model is set up for only the ER with realistic bathymetry and is run for a 2 day period with diurnal tides. The horizontal and vertical grid sizes are 250 m and 10 m for the 3D simulation.

RESULTS

Figure 1 presents the time-mean baroclinic horizontal kinetic energy $\langle HKE \rangle$ of case reWE, as well as the time-mean dissipation $\langle \varepsilon \rangle$ and the time-mean and depth integrated dissipation $\langle \varepsilon_d \rangle$. $\langle HKE \rangle$ is large near the subridges and along beams. Figure 1b and c indicate that the strongest dissipation occurs at the subridges, and the $\langle \varepsilon_d \rangle$ quickly drops by several orders of magnitude away from the subridges.

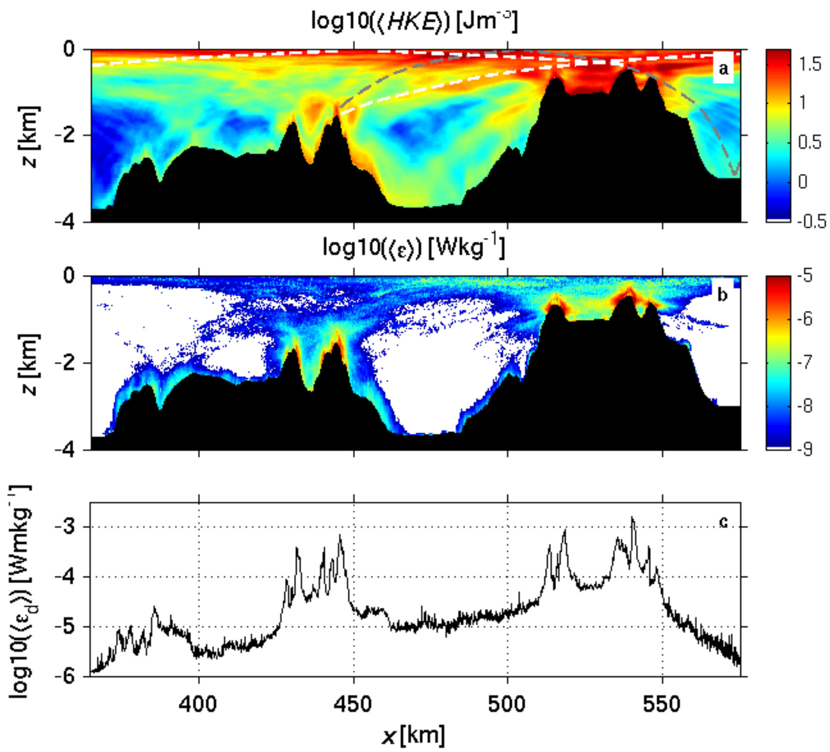

Figure 1. a) The time-mean horizontal kinetic energy is largest in the thermocline, along beams and at the ridges. The D2 beams (grey dashed lines) connect the subridges on the WR and ER, whereas the D1 beams (white dashed lines) do not connect the ridges. b) The time-mean dissipation is largest at the subridges. c) The time-mean depth-integrated dissipation also reflects this.

Figure 2 compares the results of case reWE with observations at the WR at station N2a during D2 tides. Although there are some differences in the magnitudes between the variables, the timing and physics of the data and the predictions are similar. During strong eastward barotropic flow at the WR (Figure 2f), downslope bottom velocities are enhanced and lighter water is advected below denser water, leading to dissipative overturns of up to 500 m in height (Figure 2b). The dissipation peaks as the barotropic flow relaxes. As the flow switches to the west, the depressed isopycnals rebound upslope (e.g. at t=239.6 and 240.1 days in Figure 2a) and form an upslope propagating bore that is clearly visible in the model runs. This rebound is weaker in the model than the data. The physics at station N2b are similar to station N2a. The model results are also in agreement with the data at N2b, and are not shown.

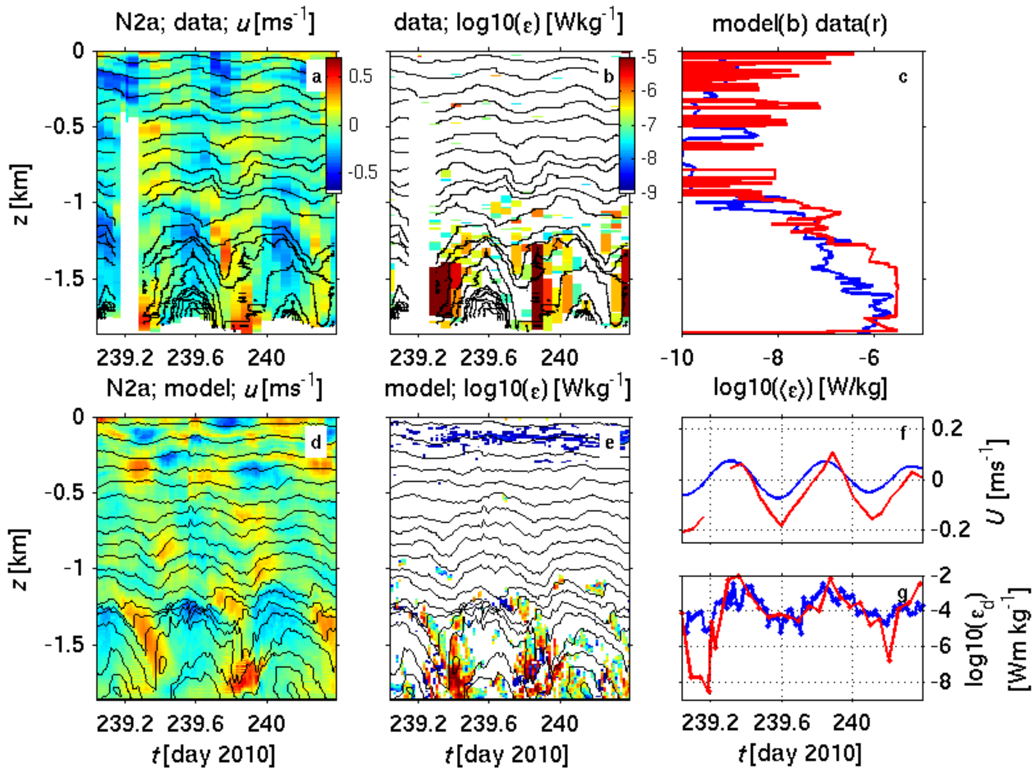

Figure 2. Model-data comparison at station N2a during D2. Observed a) zonal velocities and b) dissipation estimated from overturns. The model results are in d) and e). c) The time-mean dissipation. f) The barotropic velocities. g) The depth-integrated dissipation.

Model snapshots at maximum downslope flow at 239.9 days during N2a for case reWE in Figure 3a confirm that the observed velocities and overturns can be attributed to lee waves. A lee wave is an arrested internal wave, with phase speed equal to the velocity, barotropic and baroclinic, over at least one vertical lee-wave length above the ridge crest. All higher modes with lower wave speeds are arrested and dissipate. Station N2 is near the downslope end of the bottom attached part of the lee wave. The horizontal scales of these lee waves are O(1 km), and without good knowledge of currents and bathymetry, it may be difficult to locate the lee wave and place instruments in it. The vertical eddy viscosities with maximum values of O(1 m^2/s) in Figure 3c illustrate the dissipative nature of these lee waves. To illustrate the interaction between the ridges, a snapshot at 239.9 days of case reW (no East ridge) is plotted in Figure 3b. For station N2a the lee wave in case reW is much weaker and less turbulent than in reWE. From Figures 1 to 3 we conclude that most of the dissipation at the ridges can be attributed to high-mode turbulent lee waves and that the interaction between the WR and ER causes much stronger lee waves.

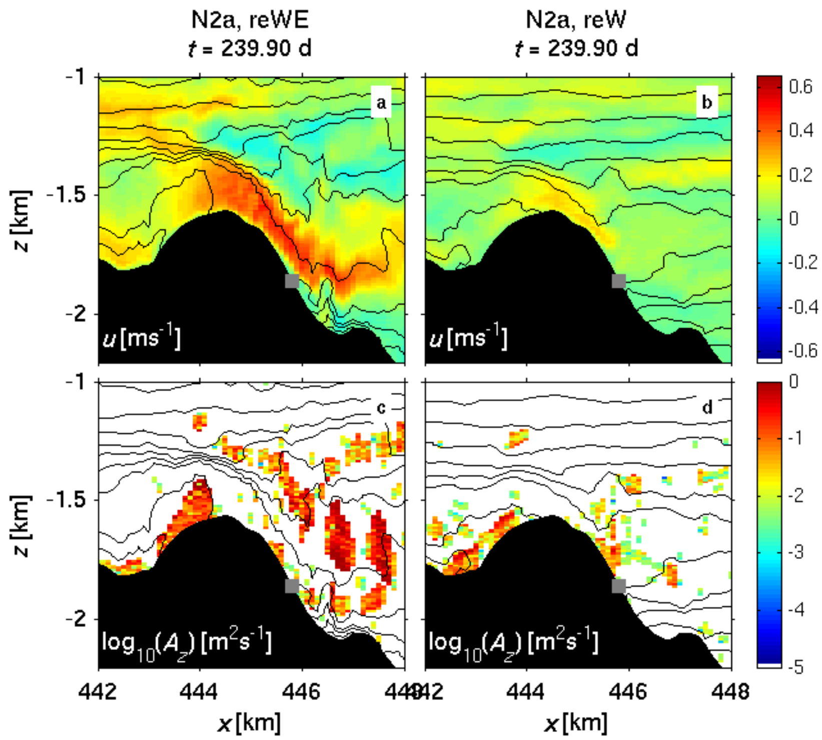

Figure 3. Snapshots of zonal velocities during strong barotropic eastward flow at the WR for a) N2a and reWE, and b) N2a and ReW (WR only). The vertical viscosities for the two cases are in c-d. The gray square marks station N2a.

We time-averaged the dissipation over periods with dominantly D2 or D1 tides and volume-integrated the dissipation about the WR, ER, and both the WR and ER (Figure 4). During D2 periods the dissipation at the WR and ER in reWE is larger than for the single ridge cases reW and reE, in agreement with Figure 3. During D1 this is also the case at the WR, while the dissipation at the ER is clearly weaker in reWE compared to reE. The causes of this D2 resonance and D1 dissonance are discussed below.

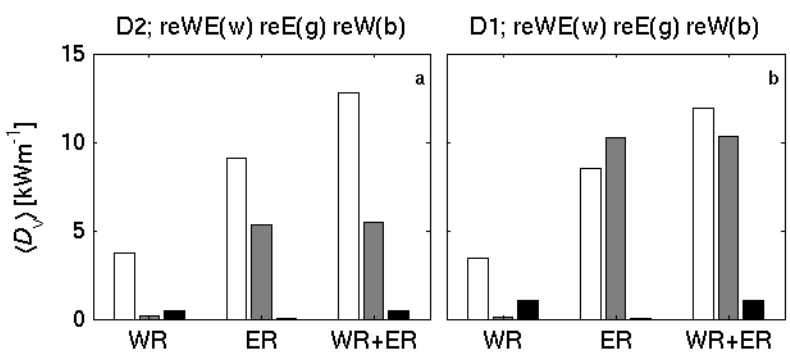

Figure 4. The time-mean dissipation, volume integrated over the WR, ER, and both the WR and ER for cases reWE (white), reE (grey), and reW (black) for a) a semidiurnal period (239.20-241.235 d) and b) a diurnal period (244.24-246.315 d).

The separation distance Δx between the tallest ridges on the WR and ER is about 90 km. This is about half of a D2 first-mode wavelength λ_2=147 km, and about a quarter of a D1 first-mode wavelength λ_1=370 km. The D2 barotropic velocities and the D2 first-mode bottom velocities are in phase at the WR and ER ridges, i.e., the resulting bottom velocities are larger in case reWE, causing larger lee waves and dissipation. In contrast, the D1 barotropic velocities and the D1 first-mode bottom velocities are out of phase at the WR and ER ridges, causing weaker velocities. Although low modes have the most energy, the superposition of the low mode velocities at the ridges does not match the stronger velocities during D2 and the weaker velocities during D1. Apparently, the near ridge velocities are also affected by the higher modes, or the baroclinic energy beams, along which internal wave energy propagates.

Some D2 and D1 beams are plotted in Figure 1a. The D2 beams connect the WR and ER, while the D1 beams do not. This connectivity provides an indication whether resonance occurs or not. We computed the D2 and D1 phases of the zonal velocities and perturbation densities for cases reW and reE, and subtracted them ($\Delta\phi_2$ and $\Delta\phi_1$). During D2, $-90^o<\Delta\phi_2<90^o$ occurs along narrow beams that connect both the subridges of the ER and the WR. These patterns are identical for the density perturbation phase differences (not shown). This is an indication that the D2 wave fields emitted from both ridges are in phase, leading to stronger velocities along the beams and at the ridge tops, not only due to linear superposition, but also due to enhanced barotropic to baroclinic conversion at the ridges that causes stronger internal waves. Conversely, the D1 velocities of reW and reE are not in phase at the WR and ER tops leading to smaller velocities and lee waves. The apparent "D1 resonance" at the WR in Figure 4 can be attributed to the resonant D2 baroclinic waves, which still have a relatively large amplitude during the D1 spring tide.

The good agreement between model and data at the 2D WR in Figure 2 supports the use of a 2D model at the WR. In contrast to the WR, the topography of the ER is much more 3D, and a 3D model may be more suitable to study the turbulence here. The ER bathymetry in Figure 5a is characterized by two north-south oriented ridges that reach up to z=-300 m that are intersected by deep channels down to z=-1000 m. Their open ends are marked c1-c4. These channels steer the barotropic currents, and they contain the bulk of the flow. The largest depth-integrated and time-mean dissipation $<\varepsilon_d>$ occurs mainly at the channel ends in Figure 5a. We also run a 2D model along the transect shown in Figure 5a. The transect's topography in Figure 5b has three large subridges, and the c3 channel is at x=108 km. $<\varepsilon_d>$ for the 2D and 3D runs is shown in Figure 5c. While in the 3D run $<\varepsilon_d>$ is largest in the channel at x=108 km, in the 2D run $<\varepsilon_d>$ is largest at the ridge crests. In the 2D model the flow is forced over the ridges, whereas in the 3D model the flow is steered by the ridges. The resulting lee waves in the 3D model are low-mode lee waves, where turbulence almost extends up to the surface. The lee wave at the channel end c2 has also been observed by Robert Pinkel and Jody Klymak in their 2011 summer cruise.

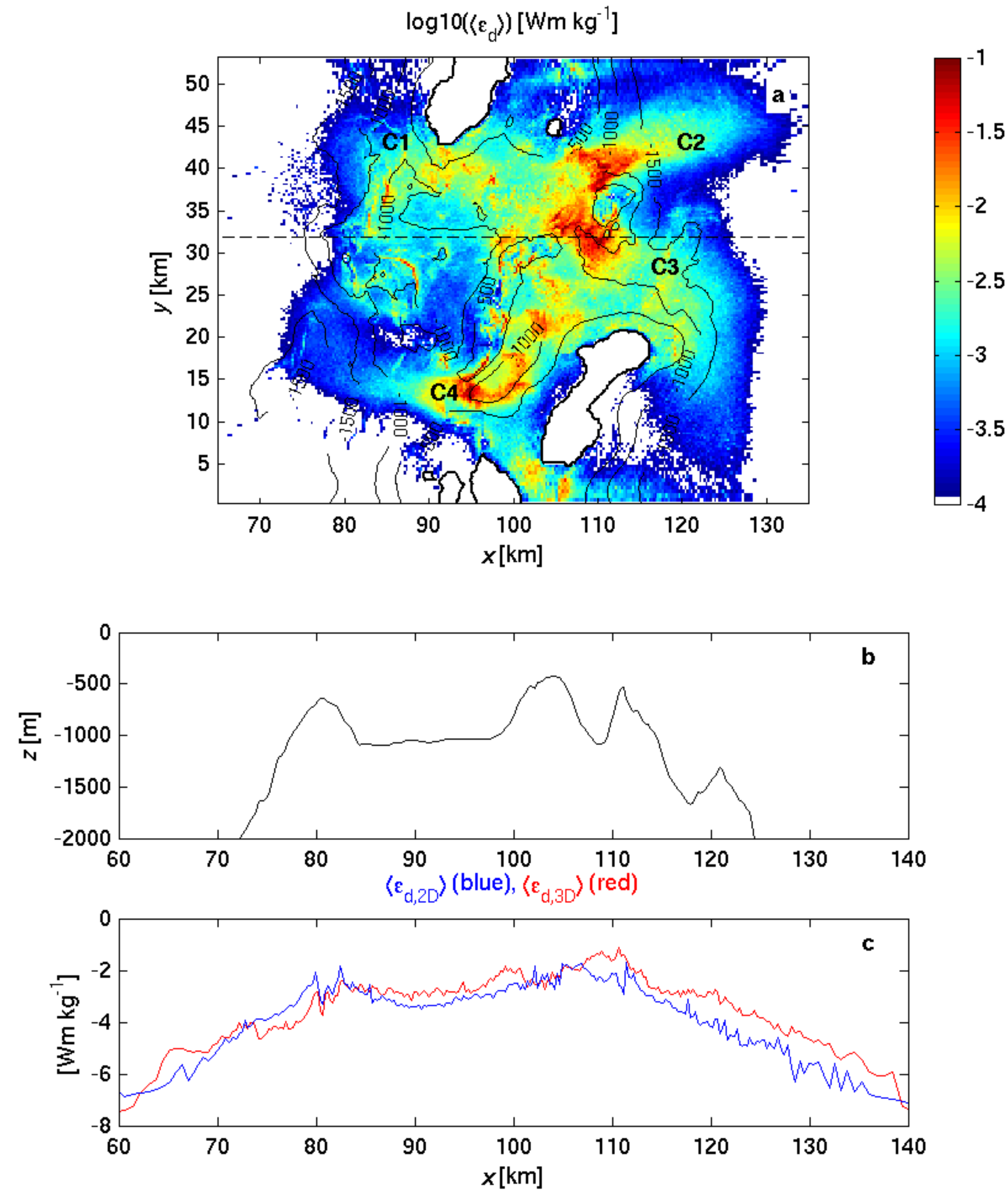

Figure 5. a) The depth-integrated and time-mean dissipation for the 3D run at the ER. The horizontal dashed line is the transect along which the 3D model is compared with the 2D model. c1-c4 mark the outflow channels. b) The bathymetry along the 2D transect. c) The depth-integrated and time-mean dissipation along this transect for the 2D model (blue) and 3D model (red). The 3D model has the largest dissipation in the channels, while the 2D model has the largest dissipation at the ridge crests.

IMPACT/APPLICATIONS

Nothing to report at present.

RELATED PROJECTS

This work is a component of the Internal Waves in Straits Experiment. We are working closely with other IWISE researchers, particularly Jody Klymak, Rob Pinkel and Matthew Alford. The work is also related to a recently proposed NSF climate process team on internal-wave driven mixing (PI Jen MacKinnon), with which Legg is collaborating.

REFERENCES

Alford, M. H., et al., 2011: Energy flux and dissipation in Luzon Strait: two tales of two ridges. J. Phys. Oceanogr., doi:10.1175/JPO-D-11-073.1.

Klymak, J. M. and S. Legg, 2010: A simple mixing scheme for models that resolve breaking internal waves. Ocean Modell., 33, 224–234.

Legg S., and J. Klymak, 2008: Internal Hydraulic Jumps and Overturning Generated by Tidal Flow over a Tall Steep Ridge. Journal of Physical Oceanography, v38, 1949-1964.